Basic three-dimensional kinematics of the vertebral column of horses walking on a treadmill

Marjan Faber, MSc; Henk Schamhardt†, PhD; René van Weeren, DVM, PhD;
Christopher Johnston, DVM, PhD; Lars Roepstorff, DVM, PhD; Ab Barneveld, DVM, PhD

Objective—To determine kinematic movements of the vertebral column of horses during normal locomotion.

Animals—5 Dutch Warmblood horses without apparent lameness or problems associated with the vertebral column.

Procedure—Kinematics of 8 vertebrae (T6, T10, T13, T17, L1, L3, L5, and S3) and both tuber coxae were determined, using bone-fixated markers. Horses were recorded while walking on a treadmill at a constant speed of 1.6 m/s.

Results—Flexion-extension was characterized by 2 periods of extension and flexion during 1 stride cycle, whereas lateral bending and axial rotation were characterized by 1 peak and 1 trough. The range of motion for flexion-extension was fairly constant for vertebrae caudal to T10 (approximately 7°). For lateral bending, the cranial thoracic vertebrae and segments in the pelvic region had the maximal amount of motion, with values of up to 5.6°. For vertebrae between T17 and L5, the amount of lateral bending decreased to < 4°. The amount of axial rotation increased gradually from 4° for T6 to 13° for the tuber coxae.

Conclusions—This direct measurement method provides 3-dimensional kinematic data for flexion-extension, lateral bending, and axial rotation of the thoracolumbar portion of the vertebral column of horses walking on a treadmill. Regional differences were observed in the magnitude and pattern of the rotations. Understanding of the normal kinematics of the vertebral column in healthy horses is a prerequisite for a better understanding of abnormal function. (*Am J Vet Res* 2000;61:399–406)

Kinematics of the vertebral column concern the kinds and amounts of motion the vertebral column makes during normal physiologic movements.[1] Vertebrae can rotate in 3 planes, resulting in **flexion-extension (FE)**, **lateral bending (LB)**, and **axial rotation (AR)**. The amount of rotation that is possible varies along the vertebral column, depending on the size, shape, and orientation of anatomic structures such as the intervertebral discs, articular facet joints, lateral joints, dorsal spinous processes, and ligaments.

There is growing interest in the kinematics of the vertebral column of horses because of the increasing prevalence of problems originating from this structure. However, fundamental information on the kinematics of the vertebral column of horses is lacking. Research to quantify kinematics of the vertebral column has primarily been performed with in vitro techniques, using isolated dissected thoracolumbar vertebral columns.[2-4] From those studies, it was concluded that the amount of rotation is limited (< 5°) for most intervertebral joints, except in the cranial thoracic joints and lumbosacral joint (> 20°).[4]

In vivo assessment of vertebral column movements is more difficult because of a number of complicating factors. First, the movements are complex and relatively small, which requires an accurate measurement technique. Second, the skin covering the vertebrae obscures direct observation and quantification of vertebral movements. And third, the mass of the epaxial muscles makes the vertebral column relatively inaccessible. Despite these problems, a number of recent studies have attempted to portray kinematics of the equine vertebral column during locomotion in vivo.[5,6] However, rotation analysis in those studies was performed only in the sagittal plane, limiting the measured movement to a description of FE. This approach can provide, at best, information on motion in the plane of projection, but it fails to completely describe vertebral motion behavior. Furthermore, in the other studies, skin-fixated markers were used, which are prone to artifacts attributable to skin movement.

In the study reported here, the thoracolumbar vertebral column and pelvic movements in all 3 dimensions were assessed in a group of clinically normal horses during walking. Markers were rigidly affixed to vertebrae by means of transcutaneously implanted Steinmann pins, preventing artifacts attributable to skin movement and allowing an accurate **3-dimensional (3-D)** analysis of the amount, type, and timing of all rotational movements in the vertebral column during locomotion.

Materials and Methods

Animals—Five Dutch Warmblood horses (4 geldings, 1 mare) were used. Horses were 2 to 4 years old, had a height (mean ± SD) of 159 ± 3 cm, and weighed 443 ± 46 kg. Before the study began, horses were accustomed to locomotion on a treadmill. Exact locations of the dorsal spinous processes of T6, T10, T13, T17, L1, L3, L5, and S3 were determined by

Received Apr 16, 1999.
Accepted Jun 8, 1999.
From the Equine Biomechanics Research Group, Departments of Equine Sciences (Faber, van Weeren, Barneveld) and Veterinary Anatomy and Physiology (Schamhardt), Faculty of Veterinary Medicine, Utrecht University, PO Box 80.153, 3508 TD Utrecht, The Netherlands; and the Equine Biomechanics Laboratory, Department of Anatomy and Histology, Swedish University of Agricultural Sciences, 750 05 Uppsala, Sweden (Johnston, Roepstorff).
The authors thank Andries Klarenbeek and Jörg Eggers for technical assistance.
†Deceased.

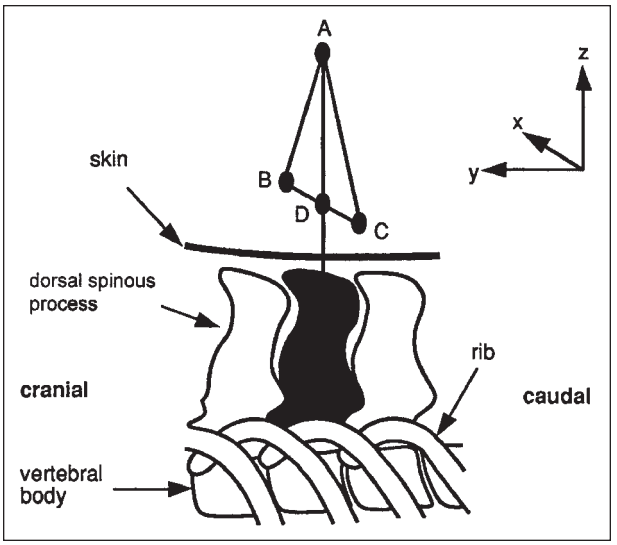

Figure 1—Illustration of the marker device attached to a vertebra and orientated in the laboratory coordinate system (x-, y-, and z-axis). Markers are indicated (A-D).

use of fluoroscopy and indicated on the skin. Positions of the left and right tuber coxae were determined by palpation.

Technique—Experimental procedures were approved by the Utrecht University Ethical Committee and were in full compliance with the Act on Animal Experiments. Horses were sedated (detomidine hydrochloride[a]; 0.01 mg/kg of body weight, IV), and previously indicated sites were prepared for surgery and infiltrated with a 2% solution of lidocaine hydrochloride.[b] A stab incision was made through the skin and underlying tissue to the underlying bones, using a No. 11 scalpel blade. A 4- to 8-cm-long, 3.0-mm-thick Steinmann pin was driven into the dorsal spinous process or tuber coxae without prior drilling. Length of the pin used was dependent on the thickness of the tissues between bone and skin; each pin protruded approximately 1 cm above the skin.

Four hours after sedation, horses were prepared for the actual measurement session. A custom-built lightweight marker device was attached to each pin. Each marker device had 4 markers attached to it; thus, each selected structure (ie, vertebrae and tuber coxae) had a set of 4 markers. The markers were lightweight reflective spherical balls, each of which was 9 mm in diameter.[c] Marker devices had the profile of the sail on a boat (**Fig 1**), consisting of an approximately equilateral triangle with a distance of 20 cm between markers. Markers were glued onto each corner of the marker devices (A, B, and C), and another marker (D) was placed midway between the 2 markers that created the base of the triangle (ie, midway between markers B and C). Additional reflective markers (30 mm in diameter) were placed on the hooves of both hind limbs. Custom-made uniaxial accelerometers were affixed to all 4 hooves.

Data collection—A commercially available system[c] was used to record positions of the markers. Seven cameras were positioned at various locations around the treadmill. Two cameras were positioned approximately 1.60 m above the ground, whereas all other cameras were approximately 2.50 m above the ground. These camera positions enabled simultaneous recording of both markers on the hooves of the hind limb and the markers placed on the vertebrae and tuber coxae. Prior to obtaining the recording, a calibration frame (1,000 × 500 × 850 mm) was positioned in such a way that the thoracolumbar portion of the vertebral column of each horse was located within the calibrated field during the data recording period. The set-up allowed measurement of marker positions with an accuracy of 0.3 mm in all 3 dimensions, provided the markers remained within the calibrated field. Both hoof markers were located outside the calibration field and, therefore, were reconstructed less accurately. This was of minor importance, because the hoof markers were used only for stride-pattern determination.

The system simultaneously recorded data of the 42 markers (4 on each of the 10 marker devices and 2 on the hooves of the hind limbs). Data for marker position and the accelerometer were collected at 240 and 3,600 Hz, respectively, during a 5-second period. Data were synchronized and stored on a personal computer for additional processing. The experimental protocol included sequential data collection while horses were walking (1.6 and 1.8 m/s), trotting (4.0 m/s), and cantering (7.0 m/s) during a single session. For this report, we considered only data obtained while horses were walking at 1.6 m/s.

Calculation of the 3-D kinematics of the vertebral column—Kinematics of the vertebral column are a combination of 3 rotations and 3 translations. In the study reported here, only the rotations were included. To describe these rotations, a standard right-handed orthogonal Cartesian coordinate system was used. In the laboratory coordinate system, the positive y-axis was directed along the line of progression. The z-axis was perpendicular to the y-axis, oriented vertically, with the positive axis in the upward direction. The x-axis was perpendicular to these 2 axes (Fig 1). Consequently, FE was defined as rotation around the x-axis, LB was defined as rotation around the z-axis, and AR was defined as rotation around the y-axis.

The 3-D spatial marker coordinates were reconstructed from the multiple 2-dimensional camera images, using a direct linear transformation procedure in the software of the commercially available recording system.[c] The 3-D marker coordinates initially were filtered by use of a second-order low-pass Butterworth filter (cutoff frequency, 10 Hz). These filtered coordinates subsequently were used to calculate the 3-D angular rotations. The calculation technique is described elsewhere.[7] Briefly, it was assumed that each horse walked in a straight line and at a constant speed on the treadmill. For 2 successive hoof contacts of 1 limb (ie, 1 stride cycle), the location of each marker ideally should have been identical. When this was not the case, a correction was performed in all 3 dimensions, based on the assumption that the difference between the initial and end position of the marker occurred gradually and was equally distributed over the entire stride cycle. Thus a linear correction factor, proportional to the point in time of the stride cycle, was calculated and subtracted from the instantaneous marker location. To calculate the rotations of each vertebra in terms of FE, LB, and AR, we developed a software program based on the algorithm described by Söderkvist and Wedin.[8] In this calculation, the reference orientation of the marker configuration was defined for each specific marker device. All other orientations during the stride cycle were correlated to that reference orientation. The reference orientation was calculated as the average orientation during the stride cycle, which assumed that the rotations were approximately symmetric. Using this process, the definition of a local coordinate system can be omitted. The reference orientation also defined the reference value for the distance between markers within each marker device. For each instant in time during the angle-calculation procedure, residuals were calculated between these reference distances and the momentary distances. Residuals were averaged for the entire stride cycle and represented the accuracy to reconstruct the position of each marker plus the rigidity of each marker device.

At that point in the analysis, diagrams of angle versus time values (ie, **angular movement patterns [AMP]**) encom-

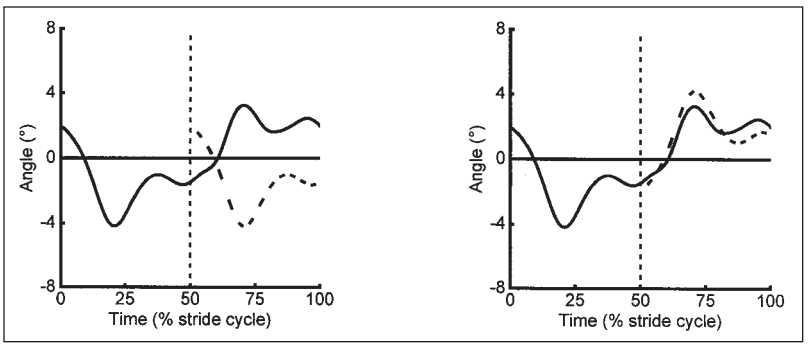

Figure 2—Illustration of the glide (left) and reflection (right) procedures applied to axial rotation data. For the glide procedure, the first half of the stride cycle is shifted to the right, to the midpoint (50%) of the stride cycle on the x-axis. Subsequently, during the reflection procedure, the shifted curve (- - -) is reflected around the x-axis. As a result, the curve of the first and second half of the stride cycle can be compared.

passed several stride cycles. To identify separate stride cycles, the starting point of each stride cycle was defined as the initial ground contact for the left hind limb. This moment in time was determined interactively by using the z-coordinate and accelerometer data of the left hind limb.[9] Each stride cycle was adjusted to 101 data points (100 intervals), with 0% being hoof contact of the left hind limb and 100% being the subsequent hoof contact for the same limb. The AMP per stride cycle were inspected visually. Stride cycles with a deviant pattern (judged by observation) or aberrant stride cycle duration (stride cycles with a duration that were outside the range defined by mean ± 2 SD) were excluded. Mean AMP were calculated for all remaining stride cycles. For all AMP, positive-slope segments indicated counter-clockwise rotations, and negative-slope segments indicated clockwise rotations.

Variability of kinematics of the vertebral column—Repeatability of the AMP was calculated for **within-horse variation (WHV**; among collected stride cycles within the same horse) and **between-horse variation (BHV**; between the mean AMP of the 5 horses). Both WHV and BHV were expressed as the **coefficient of variation (CV)**. The CV was determined by calculating a SD for each data point during the stride cycle. Subsequently, the root mean square of all SD values was expressed as a percentage of the range of motion and multiplied by 100. The CV was a measure for the exact agreement between the AMP.

Quantitative characterization of AMP—Several variables were calculated to quantitatively characterize AMP. Range of motion was calculated for the vertebral AMP as the difference between the maximum and minimum AMP values. Timing of peak amplitudes in the vertebral AMP was expressed as a percentage of the stride cycle duration. A **correlation coefficient (*R*)** was calculated between vertebral AMP as a test for the degree of rigid body behavior of successive vertebrae during locomotion. Values approaching 1 implied a rigid body behavior.

Because walking produces a symmetric gait, the motion that takes place during the first half of the stride cycle is repeated during the second half of the stride cycle.[10] To compare the first and second half of each stride cycle, a glide procedure and a reflection procedure were applied to the AMP of the LB and AR, whereas only the reflection procedure was applied to FE data (**Fig 2**). Symmetry was quantified by determining the amount of exact agreement in terms of the **root mean square of the difference as a percentage of the range of motion (SYM_{CV})** and by determining the **correlation coefficient of the amount of similarity in shape (SYM_R)**. Symmetry in the AMP resulted in a SYM_{CV} value that approached 0% and a SYM_R value that approached 1.

All results were reported as mean ± SD and were calculated for all available data for each structure. Usually, 5 AMP were available for between-horse comparisons. However, in a number of horses, marker devices became loose during the recording session and had to be removed from the vertebrae. This happened once for L3 and 3 times for L5. In 1 recording session, the device attached to the right tuber coxae could not be recorded properly, and these data were excluded from further analysis.

Results

Error analysis—Residuals of the angle calculation procedure generally were of the same order of magnitude for all selected structures, ranging from 0.36 ± 0.09 mm for the left tuber coxae to 0.57 ± 0.05 mm for L5. Because markers within the calibration field could be reconstructed to an accuracy of 0.3 mm, the measurement error was the main contributor to the residuals of the angle calculation procedure. The nonrigid behavior of the marker devices accounted for the remaining error.

Temporal variables—Three to 4 stride cycles were analyzed per horse. The 5 horses walked at a speed of 1.62 ± 0.03 m/s, and the stride cycle duration was 1.09 ± 0.08 seconds, as determined from analysis of the hoof marker data.

Variability—Consistency of vertebral AMP observed within each horse depended on the location of the structure and the type of rotation involved. For all rotations, WHV values were higher in caudal than in cranial structures. The AR was the most consistent motion, with WHV values of < 6% for all structures, except the 2 most-cranial vertebrae (T6 and T10); the WHV values for those vertebrae were 9 to 10% (**Table 1**). For FE, slightly larger WHV values were detected, with values ranging from 6 to 8% for all structures, except T6, which had a WHV value of 13.2%. The highest WHV values were found for LB, with a minimum WHV value of 7.8% and a maximum WHV value of 18.2%.

It was evident that the BHV value was 2 to 3 times higher than the WHV value for all structures and rotations (Table 1). The BHV value for FE and AR was 10 to 16%, except for T6 in which the BHV value increased to 35%. In contrast, LB had a much higher BHV value, ranging between 16 and 25% for most structures.

Exceptions were T17 and L1, which had extremely high BHV values caused by a smaller range of motion.

Vertebral flexion and extension—Vertebral FE was characterized by 2 full oscillations during each stride cycle (**Fig 3**). At the moment of hoof contact for the left hind limb, T10 was rotating clockwise, whereas the rotation of S3 was in the opposite direction. As a result, the vertebral column was extending. Motion of extension began 5 to 10% before the moment of hoof contact, and extension continued through approximately 15% of the stride cycle. A similar moment of extension of the vertebral column was evident between 40 and 65% of the stride cycle. The vertebral column flexed whenever the rotation of the cranial thoracic vertebrae and sacral vertebrae was opposite in the sense that there was counter-clockwise rotation in the thoracic region and clockwise rotation in the sacral region. This was evident during the periods from 15 to 40% and 65 to 90% of the stride cycle or approximately the period in the stride cycle when the forelimb was in contact with the ground and the ipsilateral hind limb was in the early swing phase.

Range of motion was the lowest for T6 (4.2 ± 1.6°) and increased to > 8.0° for T10 and T13. Range of motion for the vertebrae caudal to T13 were all 6.5 to 7.0° (**Table 2**). A pronounced shift in the timing of the maximum and minimum FE angle in the AMP was observed. The most-cranial thoracic vertebrae achieved a minimum FE angle in the FE movement at approximately 10 and 60% of the stride cycle. The more caudal the location of the vertebra, the earlier the minimum FE angle was reached. In the sacroiliac region, timing of the first minimum FE angle approximately coincided with hoof contact of the hind limbs (t = 0% and t = 50% for hoof contact of the left and right hind limb, respective-

Table 1—Mean ± SD values for within-horse variability (WHV) and between-horse variability (BHV) of flexion-extension (FE), lateral bending (LB), and axial rotation (AR) angular motion patterns of each vertebra and tuber coxae during walking on a treadmill

	FE		LB		AR	
Structure	**WHV**	**BHV**	**WHV**	**BHV**	**WHV**	**BHV**
Vertebra						
T6	13.2 ± 5.6	35.0	15.8 ± 9.7	33.4	9.1 ± 2.6	35.9
T10	6.2 ± 1.5	13.5	11.3 ± 2.3	23.4	9.7 ± 4.8	22.9
T13	6.0 ± 1.6	11.4	11.6 ± 4.0	23.3	5.7 ± 1.2	16.7
T17	6.2 ± 2.8	13.9	17.9 ± 6.7	100.0	4.6 ± 1.4	14.6
L1	5.9 ± 2.4	16.3	14.2 ± 5.4	62.9	4.3 ± 1.6	12.6
L3	7.4 ± 2.5	16.3	13.5 ± 4.9	35.1	4.4 ± 1.5	11.4
L5	7.6 ± 0.1	12.5	18.2 ± 0.6	16.2	5.2 ± 2.3	12.1
S3	7.8 ± 2.2	14.5	10.8 ± 5.4	24.9	4.1 ± 2.0	11.2
Tuber coxae						
Left	6.9 ± 2.2	14.5	9.8 ± 4.1	24.9	4.6 ± 1.6	11.2
Right	6.6 ± 1.0	18.6	7.8 ± 2.6	21.1	3.4 ± 0.6	10.1

Values are expressed as the coefficient of variation in percentage of the range of motion.

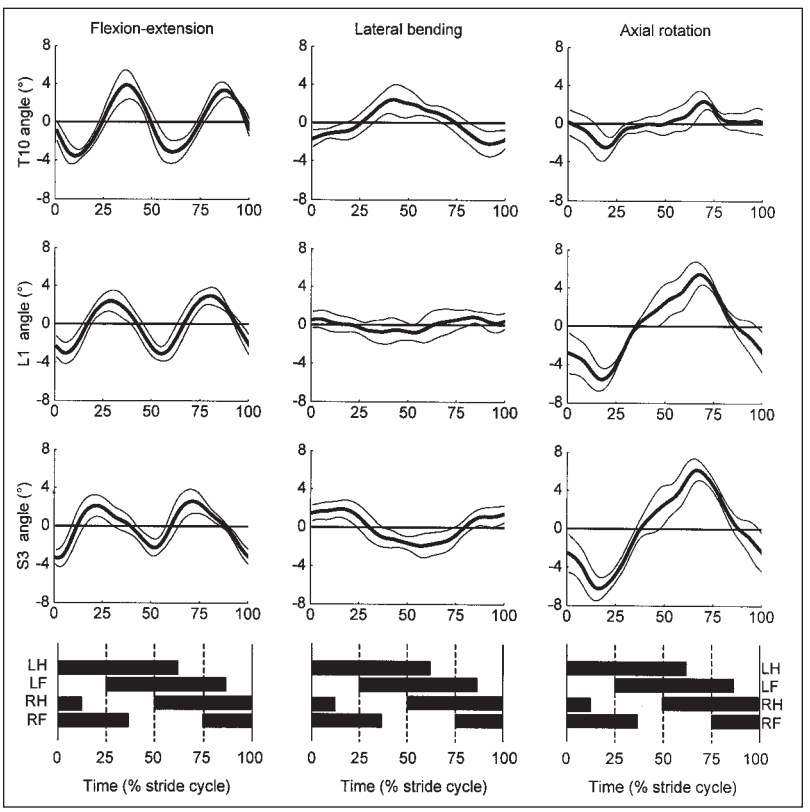

Figure 3—Mean (thick line) ± SD (thin lines) values for each of the 3 vertebral angular motion patterns during 1 complete stride cycle for 5 horses walking on a treadmill (1.6 m/s). The stride cycle starts with the moment of hoof contact of the left hind limb. For each rotation, results for 3 vertebrae (T10, L1, and S3) are provided. Horizontal bars indicate the stance phase for each limb. LH = Left hind limb. LF = Left forelimb. RH = Right hind limb. RF = Right forelimb.

ly). Thus, there was a time shift of 10% for the minimum FE angle (**Fig 4**). For the maximum FE angle, a similar time shift was seen, but those values were shifted 15%.

The amount of intravertebral symmetry, evaluated by comparing AMP during the first and second half of the stride cycle, was not high. The SYM_{CV} ranged from 9.5 ± 5.4 to 16.6 ± 9.2% (**Table 3**), and SYM_R ranged from 0.80 ± 0.19 to 0.97 ± 0.03 (**Table 4**). It should be mentioned that the degree of symmetry varied widely among horses. In general, a higher degree of symmetry was found in vertebrae between T10 and L5.

The FE AMP of L1 through S3 and both tuber coxae had a high correlation, indicating that these vertebrae moved simultaneously and behaved as a single rigid body. For the remaining thoracic vertebrae, AMP tended to be highly correlated ($R > 0.95$) between adjacent vertebrae. This correlation decreased rapidly for vertebrae located farther apart (**Table 5**).

Vertebral lateral bending—During walking, the LB was a single periodic motion (Fig 3). As such, T10 rotated opposite to S3, whereas L1 hardly had any LB. The LB AMP of T6 had a distinct moment of maximum and minimum LB angle. These moments were evident just before the moment of hoof contact for the hind limb. For the sacral vertebrae, the maximum and minimum LB angle were not that obvious, because the position of the maximum and minimum LB angle is sustained during a period of 10 to 20% of the stride cycle. Long before the moment of hoof contact for the left hind limb, the pelvic region started to bend toward that side, resulting in a positive-slope segment in the AMP. Simultaneously, the cranial thoracic vertebrae had an opposite clockwise rotation. As a result, the vertebral column had a convex bend toward the contralateral side. The point of reversal, existing between the thoracic and pelvic region, had a limited amount of LB. The location of the point of reversal was usually detected at approximately the thoracolumbar junction, but there was variability among horses.

Range of motion for LB differed along the vertebral column (Table 2). In the caudal thoracic and cranial lumbar region, range of motion was < 3°, whereas range of motion was as high as 6° in the pelvic region.

Symmetry of the intravertebral pattern for LB was

Table 2—Mean ± SD values for vertebral range of motion (°) for FE, LB, and AR of each vertebra and tuber coxae

Structure	FE	LB	AR
Vertebra			
T6	4.2 ± 1.6	4.1 ± 1.5	4.3 ± 1.2
T10	8.1 ± 1.7	5.3 ± 2.3	5.3 ± 2.3
T13	8.5 ± 1.9	4.6 ± 2.1	8.4 ± 2.2
T17	7.1 ± 2.2	2.6 ± 0.9	11.0 ± 2.7
L1	7.0 ± 1.5	3.3 ± 0.8	11.3 ± 2.4
L3	6.6 ± 1.3	3.7 ± 1.0	11.4 ± 2.7
L5	6.5 ± 1.2	3.7 ± 0.1	13.1 ± 1.2
S3	6.8 ± 1.3	4.9 ± 1.3	12.6 ± 2.5
Tuber coxae			
Left	7.3 ± 1.4	5.1 ± 1.7	13.0 ± 2.7
Right	6.9 ± 1.2	5.6 ± 1.4	12.8 ± 2.8

Table 3—Mean ± SD values for the symmetry of the intravertebral pattern expressed as the coefficient of variation in percentage of the range of motion for FE, LB, and AR of each vertebra and tuber coxae

Structure	FE	LB	AR
Vertebra			
T6	15.7 ± 5.4	19.1 ± 8.9	10.8 ± 6.0
T10	8.7 ± 3.8	10.3 ± 5.7	8.2 ± 3.9
T13	8.4 ± 4.3	14.0 ± 9.3	6.0 ± 2.6
T17	10.9 ± 3.6	13.5 ± 1.9	3.8 ± 2.0
L1	12.8 ± 4.4	21.4 ± 16.5	3.1 ± 1.8
L3	10.7 ± 3.4	16.9 ± 12.8	3.5 ± 1.7
L5	9.5 ± 5.4	12.8 ± 0.9	4.8 ± 2.1
S3	15.4 ± 8.6	14.4 ± 9.2	2.3 ± 0.9
Tuber coxae			
Left	16.6 ± 9.2	11.1 ± 8.0	3.4 ± 1.7
Right	14.4 ± 6.1	11.3 ± 8.7	3.8 ± 1.1

Table 4—Mean ± SD values for the symmetry of the intravertebral pattern expressed as the correlation coefficient for FE, LB, and AR of each vertebra and tuber coxae

Structure	FE	LB	AR
Vertebra			
T6	0.81 ± 0.20	0.76 ± 0.24	0.84 ± 0.16
T10	0.97 ± 0.02	0.94 ± 0.05	0.92 ± 0.07
T13	0.97 ± 0.03	0.84 ± 0.23	0.96 ± 0.04
T17	0.94 ± 0.05	0.78 ± 0.21	0.99 ± 0.01
L1	0.91 ± 0.06	0.24 ± 0.86	0.99 ± 0.02
L3	0.94 ± 0.04	0.64 ± 0.58	0.99 ± 0.01
L5	0.95 ± 0.05	0.91 ± 0.04	0.99 ± 0.00
S3	0.83 ± 0.19	0.84 ± 0.20	1.00 ± 0.00
Tuber coxae			
Left	0.80 ± 0.19	0.90 ± 0.13	0.99 ± 0.01
Right	0.93 ± 0.05	0.92 ± 0.13	0.99 ± 0.01

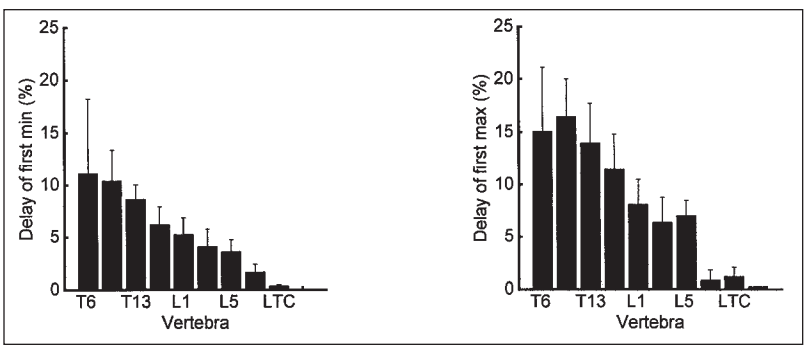

Figure 4—Graph of the time delay across the thoracolumbar portion of the vertebral column for the first minimum (min; left) and maximum (max; right) of the flexion-extension movement pattern in the stride cycle. Time delay was calculated with respect to the first vertebra that reached the minimum and maximum, respectively, during the stride cycle. LTC = Left tuber coxae.

Table 5—Symmetry of the intervertebral pattern of vertebral angular motion patterns for FE, expressed as mean ± SD of the coefficient of correlation between the angular motion patterns of successive vertebrae and the tuber coxae

Structure	T6	T10	T13	T17	L1	L3	L5	S3	Left tuber coxae	Right tuber coxae
T6	—	0.78 ± 0.19	0.70 ± 0.28	0.55 ± 0.53	0.49 ± 0.59	0.30 ± 0.69	0.27 ± 0.89	0.19 ± 0.66	0.13 ± 0.65	–0.01 ± 0.69
T10	0.78 ± 0.19	—	0.96 ± 0.04	0.74 ± 0.22	0.58 ± 0.27	0.43 ± 0.38	0.39 ± 0.43	0.03 ± 0.40	–0.06 ± 0.40	–0.17 ± 0.45
T13	0.70 ± 0.28	0.96 ± 0.04	—	0.88 ± 0.09	0.75 ± 0.14	0.64 ± 0.23	0.56 ± 0.25	0.21 ± 0.31	0.12 ± 0.31	0.05 ± 0.38
T17	0.55 ± 0.53	0.74 ± 0.22	0.88 ± 0.09	—	0.95 ± 0.03	0.91 ± 0.06	0.88 ± 0.09	0.58 ± 0.14	0.50 ± 0.15	0.46 ± 0.18
L1	0.49 ± 0.59	0.58 ± 0.27	0.75 ± 0.14	0.95 ± 0.03	—	0.98 ± 0.02	0.98 ± 0.02	0.74 ± 0.06	0.66 ± 0.08	0.64 ± 0.06
L3	0.30 ± 0.69	0.43 ± 0.38	0.64 ± 0.23	0.91 ± 0.06	0.98 ± 0.02	—	0.98 ± 0.01	0.83 ± 0.07	0.75 ± 0.10	0.74 ± 0.08
L5	0.27 ± 0.89	0.39 ± 0.43	0.56 ± 0.25	0.88 ± 0.09	0.98 ± 0.02	0.98 ± 0.01	—	0.84 ± 0.00	0.78 ± 0.03	0.78 ± 0.00
S3	0.19 ± 0.66	0.03 ± 0.40	0.21 ± 0.31	0.58 ± 0.14	0.74 ± 0.06	0.83 ± 0.07	0.84 ± 0.00	—	0.98 ± 0.01	0.98 ± 0.01
Left tuber coxae	0.13 ± 0.65	–0.06 ± 0.40	0.12 ± 0.31	0.50 ± 0.15	0.66 ± 0.08	0.75 ± 0.10	0.78 ± 0.03	0.98 ± 0.01	—	0.96 ± 0.01
Right tuber coxae	–0.01 ± 0.69	–0.17 ± 0.45	0.05 ± 0.38	0.46 ± 0.18	0.64 ± 0.06	0.74 ± 0.08	0.78 ± 0.00	0.98 ± 0.01	0.96 ± 0.01	—

— = Not determined.

Table 6—Symmetry of the intervertebral pattern of vertebral angular motion patterns for LB, expressed as mean ± SD of the coefficient of correlation between the angular motion patterns of successive vertebrae and the tuber coxae

Structure	T6	T10	T13	T17	L1	L3	L5	S3	Left tuber coxae	Right tuber coxae
T6	—	0.76 ± 0.25	0.54 ± 0.20	–0.19 ± 0.59	–0.42 ± 0.50	–0.65 ± 0.37	–0.41 ± 0.31	–0.55 ± 0.35	–0.53 ± 0.36	–0.51 ± 0.41
T10	0.76 ± 0.25	—	0.85 ± 0.16	0.08 ± 0.77	–0.24 ± 0.66	–0.63 ± 0.38	–0.65 ± 0.09	–0.74 ± 0.24	–0.74 ± 0.19	–0.81 ± 0.17
T13	0.54 ± 0.20	0.85 ± 0.16	—	0.38 ± 0.53	0.00 ± 0.54	–0.37 ± 0.29	–0.51 ± 0.30	–0.56 ± 0.32	–0.57 ± 0.24	–0.68 ± 0.25
T17	–0.19 ± 0.59	0.08 ± 0.77	0.38 ± 0.53	—	0.77 ± 0.14	0.62 ± 0.29	0.10 ± 0.66	0.21 ± 0.65	0.23 ± 0.60	0.07 ± 0.72
L1	–0.42 ± 0.50	–0.24 ± 0.66	0.00 ± 0.54	0.77 ± 0.14	—	0.85 ± 0.19	0.23 ± 0.28	0.40 ± 0.55	0.44 ± 0.49	0.35 ± 0.63
L3	-0.65 ± 0.37	–0.63 ± 0.38	–0.37 ± 0.29	0.62 ± 0.29	0.85 ± 0.19	—	0.73 ± 0.01	0.81 ± 0.15	0.85 ± 0.12	0.83 ± 0.16
L5	–0.41 ± 0.31	–0.65 ± 0.09	–0.51 ± 0.30	0.10 ± 0.66	0.23 ± 0.28	0.73 ± 0.01	—	0.91 ± 0.10	0.96 ± 0.05	0.91 ± 0.00
S3	–0.55 ± 0.35	–0.74 ± 0.24	–0.56 ± 0.32	0.21 ± 0.65	0.40 ± 0.55	0.81 ± 0.15	0.91 ± 0.10	—	0.97 ± 0.05	0.98 ± 0.02
Left tuber coxae	–0.53 ± 0.36	–0.74 ± 0.19	–0.57 ± 0.24	0.23 ± 0.60	0.44 ± 0.49	0.85 ± 0.12	0.96 ± 0.05	0.97 ± 0.05	—	0.98 ± 0.03
Right tuber coxae	–0.51 ± 0.41	–0.81 ± 0.17	–0.68 ± 0.25	0.07 ± 0.72	0.35 ± 0.63	0.83 ± 0.16	0.91 ± 0.00	0.98 ± 0.02	0.98 ± 0.03	—

See Table 5 for key.

Table 7—Symmetry of the intervertebral pattern of vertebral angular motion patterns for AR, expressed as mean ± SD of the coefficient of correlation between the angular motion patterns of successive vertebrae and the tuber coxae

Structure	T6	T10	T13	T17	L1	L3	L5	S3	Left tuber coxae	Right tuber coxae
T6	—	0.63 ± 0.21	0.31 ± 0.53	0.18 ± 0.50	0.13 ± 0.55	0.02 ± 0.58	0.36 ± 0.21	0.14 ± 0.58	0.13 ± 0.59	0.11 ± 0.67
T10	0.63 ± 0.21	—	0.87 ± 0.18	0.78 ± 0.22	0.75 ± 0.27	0.67 ± 0.29	0.83 ± 0.16	0.72 ± 0.30	0.71 ± 0.32	0.71 ± 0.36
T13	0.31 ± 0.53	0.87 ± 0.18	—	0.97 ± 0.03	0.95 ± 0.05	0.93 ± 0.06	0.93 ± 0.08	0.94 ± 0.06	0.93 ± 0.07	0.95 ± 0.04
T17	0.18 ± 0.50	0.78 ± 0.22	0.97 ± 0.03	—	0.98 ± 0.03	0.98 ± 0.03	0.99 ± 0.00	0.97 ± 0.04	0.97 ± 0.05	0.97 ± 0.05
L1	0.13 ± 0.55	0.75 ± 0.27	0.95 ± 0.05	0.98 ± 0.03	—	0.99 ± 0.01	0.99 ± 0.01	0.99 ± 0.01	0.99 ± 0.01	0.99 ± 0.01
L3	0.02 ± 0.58	0.67 ± 0.29	0.93 ± 0.06	0.98 ± 0.03	0.99 ± 0.01	—	0.99 ± 0.00	1.00 ± 0.00	0.99 ± 0.00	0.99 ± 0.00
L5	0.36 ± 0.21	0.83 ± 0.16	0.93 ± 0.08	0.99 ± 0.00	0.99 ± 0.01	0.99 ± 0.00	—	0.99 ± 0.01	0.99 ± 0.01	0.98 ± 0.00
S3	0.14 ± 0.58	0.72 ± 0.30	0.94 ± 0.06	0.97 ± 0.04	0.99 ± 0.01	1.00 ± 0.00	0.99 ± 0.01	—	1.00 ± 0.00	1.00 ± 0.00
Left tuber coxae	0.13 ± 0.59	0.71 ± 0.32	0.93 ± 0.07	0.97 ± 0.05	0.99 ± 0.01	0.99 ± 0.00	0.99 ± 0.01	1.00 ± 0.00	—	0.99 ± 0.00
Right tuber coxae	0.11 ± 0.67	0.71 ± 0.36	0.95 ± 0.04	0.97 ± 0.05	0.99 ± 0.01	0.99 ± 0.00	0.98 ± 0.00	1.00 ± 0.00	0.99 ± 0.00	—

See Table 5 for key.

low. The SYM_{CV} was 10 to 15% for most vertebrae, except for T6, L1, and L3 (Table 3) in which the values were higher (up to 21%). The SYM_R ranged from 0.24 ± 0.86 for L1 to 0.94 ± 0.05 for T10 (Table 4).

Pelvic segments (ie, S3 and both tuber coxae) moved as a single segment for LB, as indicated by a strong correlation between all AMP of these segments (**Table 6**). None of the other groups of vertebrae could be considered to move as rigid bodies; each vertebra moved independently. Negative correlations that were found for many correlations among vertebrae were caused by the opposite rotation of these vertebrae toward each other.

Vertebral axial rotation—One complete oscillation took place during 1 stride cycle for the axial rotation (Fig 3). The AMP for all vertebrae had a similar shape, with an increase in range of motion when progressing in a cranial to caudal direction (4.3 ± 1.2° to 13.1 ± 1.2°; Table 2). At the moment of hoof contact for the left hind limb, all vertebrae rotated away from that side. For all vertebrae, except T6, the minimal value was reached between 15 and 20% of the stride cycle. Subsequently during the stride cycle, the vertebrae rotated away from the contralateral side. In other words, immediately after the right hind limb lifted off the ground, which was at approximately 13% of the stride cycle, the vertebral column rotated around the longitudinal axis away from the unsupported right side. At approximately the moment that the left hind limb lifted off the ground (63% of stride cycle), the rotation reversed again away from the left side, which, from that point on, was the unsupported side.

Amount of symmetry in the AMP was high. Except for T6, T10, and T13, values for SYM_{CV} did not exceed

5% (Table 3). Similarly, values for SYM_R were ≥ 0.99 (Table 4).

For AR, vertebrae from T13 to the pelvis moved as a single segment, which was concluded on the basis of the highly correlated AMP ($R \geq 0.93$; **Table 7**). Apparently, for the AR rotation, all vertebrae from T13 to the pelvis moved as a rigid body, with a gradually increasing range of motion from cranial toward caudal and with the thoracic region nearest the fore limbs acting as a point of rotation.

Discussion

In the study reported here, we used an invasive direct measurement method to evaluate 3-D kinematics of the vertebral column of horses walking on a treadmill. The horses tolerated the entire procedure well. Pins could be positioned in the standing sedated horses without the use of any additional form of restraint. During locomotion, signs of discomfort or lameness were not observed. After finishing data collection, pins were removed, and skin incisions were closed with a single suture. These small wounds healed within several days by primary intention.

In the calculation of 3-D kinematics of the vertebral column from marker-position data, it was assumed that the local vertebral coordinate system was orientated such that FE, LB, and AR occurred along the transverse, vertical, and longitudinal axes of the laboratory coordinate system, respectively. Consequently, a horse should have moved parallel to the longitudinal axis. Whenever a horse was not walking parallel to this axis, a linear correction was used to realign the laboratory coordinate system with the vertebral coordinate system. This noticeably improved the data, and the stride cycles appeared comparable after realignment. As an alternative, Stokes et al[11] selected stride cycles for analysis that did not have appreciable bilateral or cranial-caudal drift. This was not possible in our study because of the insufficient number of stride cycles that met all criteria.

An additional assumption in the calculation technique was that the marker device and its components (ie, Steinmann pin and vertebra) behaved like a rigid body; however, a number of sources affecting the rigidity should be considered. First, the marker device was lightweight and sturdy but not perfectly rigid. Supported by results of the error analysis, it could be concluded that error introduced by nonrigid behavior of the marker device was negligible. Second, pins may bend, causing oscillations of the pin-marker device combination. Nevertheless, it was determined that the resonance frequency was considerably higher than the maximal frequency apparent in marker movement during locomotion. The third possible source of error was from motions within the vertebra-pin interface. Whenever a pin became loose, all data of the corresponding vertebra were discarded from further analysis.

On the basis of in vitro studies, it is known that the intervertebral range of mobility varies along the length of the thoracolumbar vertebral column in horses, depending on the anatomy of the intervertebral joint complexes.[2-4] Articular facet joints, tangentially orientated in the thoracic region, limit the amount of FE in the thoracic region to 2 to 4°.[12] On the other hand, facet joints in the lumbar region have a radial orientation and subsequently limit the amount of AR in that region to 1 to 2°. Transverse processes limit the amount of LB, especially when there are lateral joints between the transverse processes.[13] These lateral joints most often begin to appear at the joint between L4 and L5 and always are evident in the joints between L5-L6 and L6-S1. In 59% of the cases, these joints are fused and intervertebral movement is virtually impossible.[12] Finally, dorsal spinous processes are oriented in such a way that there is limited room for FE for all intervertebral joints, except for the lumbosacral articulation. In addition to anatomic vertebral constraints, ribs limit the amount of AR cranial to T9.[3] Despite these movement constraints, the maximal amount of AR and LB possible in vitro is ± 5° for AR and ± 11° for LB in the T10 to T12 region.[4] For the lumbosacral joint, the greatest amount of FE mobility observed was 8 to 9°.[4]

Intervertebral mobility determined in vitro cannot be applied unconditionally to in vivo vertebral column kinematics. First, for in vitro experiments, the vertebral column is isolated, missing much of the effects of soft tissue, preloads, and muscle action.[14] Furthermore, range of motion values obtained in vitro are of limited use, primarily because the end-range mobility is determined. During locomotion, these end-range values likely will not be attained. Furthermore, the manner in which loads are applied to the vertebral column is critical and can account for differences among studies.[4] Finally, the effects of isolation of the vertebral column on mobility characteristics are not known.[4,15]

Results obtained during in vitro studies usually provide ranges of motion of 1 vertebra relative to an adjacent vertebra. In our study, angular mobility was determined in terms of the absolute motion of specific vertebrae. To compare results of in vitro studies with our findings, intervertebral mobility was determined by subtracting the AMP of 2 successive vertebrae equipped with a marker device. In so doing, maximal intervertebral range of motion was between T6 and T10 for FE (5.6 ± 2.0°), between T13 and T17 for LB (4.3 ± 1.2°), and between T6 and T10 for AR (3.7 ± 0.6°). However, these intervertebral rotations include several (2, 3, or 4) intervertebral joints, because not all vertebrae were equipped with markers as a result of practical considerations. This still precludes an exact comparison with results of in vitro studies. Nevertheless, regions with maximal AR and LB mobility are similar, although the magnitudes of range of motion in vivo during walking are considerably smaller after correction for the number of intervertebral joints. According to analysis of our data for all 3 rotations, only a small fraction of the possible range of movement, based on anatomy of the vertebrae, actually is used during walking. For example, it was evident that FE for the lumbosacral joint did not exceed the range of motion in the other joints, whereas the possible range of movement in the lumbosacral joint exceeds by far that of all other intervertebral joints.[4]

In healthy horses that are not lame, the vertebral column does not move symmetrically during walking. Intravertebral symmetry of the AMP in our group of horses was close to perfect for AR of the vertebrae cau-

dal to T13, with values for $SYM_R \geq 0.99$ and $SYM_{CV} < 5\%$. However, for the remaining rotations and vertebrae, the AMP were not symmetric. This finding is in agreement with results from other equine locomotion studies. In one study in which a value of 100% corresponded to perfect symmetry,[d] symmetry values ranged from 92 to 97% for displacement patterns of trunk markers in a group of 13 horses that were not lame. In another study in which a value of 1 corresponded to perfect symmetry,[16] movement of the head, spinous process of T6, and tuber sacrale revealed symmetry indices ranging from 0.95 to 1.06 in a group of 11 horses that were not lame.

Movements of the vertebral column and hind limbs are closely associated. The direct linkage between the hind limbs and vertebral column (ie, sacroiliac joint) allows only a small amount of mobility. An indication that FE motion was generated by the hind limbs comes from the pronounced shift in the timing of the minimum and maximum values when the caudal and cranial vertebrae were compared. Extreme positions in the pelvic region were reached 10 to 15% earlier in the stride cycle, compared with the cranial thoracic vertebrae. Also, in kinematics of the vertebral column in humans, patterns have been described in which the caudal vertebrae start to rotate and the cranial vertebrae subsequently follow. This was explained as a mechanism for conservation of angular momentum generated by the limbs.[17] For AR, rotations of the thoracolumbar vertebrae were linked to the pelvic AR and, subsequently, to hind limb placement, because our results revealed a high correlation between AR AMP of the specific vertebrae. Because the forelimbs act as a pivot point, the decreasing amount of AR in the vertebrae detected from caudal to cranial can be explained. The limited amount of LB provides a more optimal transmission for cranial direction of the forward momentum generated by the hind limbs.[18] Evidence in our study for the primary role of the hind limbs in generating motion in the vertebral column during locomotion are in agreement with results obtained in cats.[19] In experiments that used electromyography in addition to a kinematic analysis, results suggested that the primary role of the muscles associated with the vertebral column during walking is to control the stiffness of the animal's vertebral column, rather than to induce movements. This leaves external forces as a source for generating motion in the vertebral column. Insufficient data are available on trunk muscular activity in horses during walking to support this hypothesis.

To our knowledge, this is the first comprehensive in vivo study on 3-D kinematics of the thoracolumbar vertebral column of horses. An understanding of the fundamental kinematics of the various segments of the vertebral column and physiologic variations therein is a prerequisite for the quantitative study of abnormalities of motion of the vertebral column and for objective evaluation of the numerous treatments that are advised for affected animals. It is understood that for a wider and possibly clinical application of kinematic analysis of the vertebral column of horses, a noninvasive technique will have to be developed that allows an accurate assessment of the 3 rotations.

[a]Domosedan, Orion Corp, Espoo, Finland.
[b]Lidocaine HCl 2%, Apharmo, Arnhem, The Netherlands.
[c]ProReflex, Qualysis, Sävedalen, Sweden.
[d]Audigié F, Pourcelot P, Degueurce C, et al. Kinematic analysis of limb and trunk motion symmetry in equine lameness (abstr), *J Biomech* 1998;(*suppl* 1):121.

References

1. White AA, Panjabi MM. The basic kinematics of the human spine. A review of past and current knowledge. *Spine* 1978;3:12–20.
2. Denoix JM. Kinematics of the thoracolumbar spine of the horse during dorsoventral movements: a preliminary report, in *Proceedings*. 2nd Int Conf Equine Exercise Physiol 1986;607–614.
3. Jeffcott LB, Dalin G. Natural rigidity of the horse's backbone. *Equine Vet J* 1980;12:101–108.
4. Townsend HG, Leach DH, Fretz PB. Kinematics of the equine thoracolumbar spine. *Equine Vet J* 1983;15:117–122.
5. Audigié F, Pourcelot PCD, Denoix JM, et al. Kinematics of the equine back: flexion-extension movements in sound trotting horses. *Equine Vet J* 1999;(*suppl* 30):210–213.
6. Pourcelot P, Audigié F, Degueurce C, et al. Kinematics of the equine back: a method to study the thoracolumbar flexion-extension movements at the trot. *Vet Res* 1998;29:519–525.
7. Faber MJ, Schamhardt HC, van Weeren PR. Determination of 3D spinal kinematics without defining a local vertebral coordinate system. *J Biomech* 1999;12:1355–1358.
8. Söderkvist I, Wedin PA. Determining the movements of the skeleton using well-configured markers. *J Biomech* 1993;26:1473–1477.
9. Schamhardt HC, Merkens HW. Objective determination of ground contact of equine limbs at the walk and trot: comparison between ground reaction forces, accelerometer data and kinematics. *Equine Vet J* 1994;(*suppl* 17):75–79.
10. Gray J. Mammals. In: Gray J, eds. *Animal locomotion*. London: Weidenfeld & Nicholson, 1968;241–298.
11. Stokes VP, Andersson C, Forssberg H. Rotational and translational movement features of the pelvis and thorax during adult human locomotion. *J Biomech* 1989;22:43–50.
12. Townsend HG, Leach DH. Relationship between intervertebral joint morphology and mobility in the equine thoracolumbar spine. *Equine Vet J* 1984;16:461–465.
13. Krüger W. Die Arbeit des Rückens. In: Krüger W, eds. *Die Fortbewegung des Pferdes*. Berlin: Verlag Paul Parey, 1939;48–62.
14. Schendel MJ, Dekutoski MB, Ogilvie JW, et al. Kinematics of the canine lumbar intervertebral joint. An in vivo study before and after adjacent instrumentation. *Spine* 1995;20:2555–2564.
15. Adams MA. Mechanical testing of the spine. An appraisal of methodology, results, and conclusions. *Spine* 1995;20:2151–2156.
16. Buchner HH, Savelberg HH, Schamhardt HC, et al. Head and trunk movement adaptations in horses with experimentally induced fore- or hindlimb lameness. *Equine Vet J* 1996;28:71–76.
17. Crosbie J, Vachalathiti R, Smith R. Patterns of spinal motion during walking. *Gait & Posture* 1997;5:6–12.
18. Rooney JR. The vertebral column. In: Rooney JR, eds. *Biomechanics of lameness in horses*. Baltimore: The Williams & Wilkins Co, 1969;90–95.
19. Carlson H, Halbertsma J, Zomlefer M. Control of the trunk during walking in the cat. *Acta Physiol Scand* 1979;105:251–253.